Experimental and numerical studies of nonlinear ultrasonic responses on plastic deformation in weld joints*

Yan-Xun Xiang(项延训)[1], Wu-Jun Zhu(朱武军)[1], Ming-Xi Deng(邓明晰)[2], and Fu-Zhen Xuan(轩福贞)[1,†]

[1] *Key Laboratory of Pressure Systems and Safety of Ministry of Education, School of Mechanical and Power Engineering, East China University of Science and Technology, Shanghai* 200237, *China*

[2] *Department of Physics, Logistics Engineering University, Chongqing* 400016, *China*

(Received 31 July 2015; revised manuscript received 7 September 2015; published online 20 December 2015)

The experimental measurements and numerical simulations are performed to study ultrasonic nonlinear responses from the plastic deformation in weld joints. The ultrasonic nonlinear signals are measured in the plastic deformed 30Cr2Ni4MoV specimens, and the results show that the nonlinear parameter monotonically increases with the plastic strain, and that the variation of nonlinear parameter in the weld region is maximal compared with those in the heat-affected zone and base regions. Microscopic images relating to the microstructure evolution of the weld region are studied to reveal that the change of nonlinear parameter is mainly attributed to dislocation evolutions in the process of plastic deformation loading. Meanwhile, the finite element model is developed to investigate nonlinear behaviors of ultrasonic waves propagating in a plastic deformed material based on the nonlinear stress–strain constitutive relationship in a medium. Moreover, a pinned string model is adopted to simulate dislocation evolution during plastic damages. The simulation and experimental results show that they are in good consistency with each other, and reveal a rising acoustic nonlinearity due to the variations of dislocation length and density and the resulting stress concentration.

Keywords: ultrasonic nonlinearity, second harmonics, plastic deformation, finite element modeling

PACS: 43.25.+y, 62.20.–x, 81.70.Cv **DOI:** 10.1088/1674-1056/25/2/024303

1. Introduction

Weld joints have been widely applied in pressure vessels, power plants, petrochemical industry, etc., which usually experience plastic damage, micro-crack initiation and growth due to the harsh service conditions in practice. Premature failures at weld joints have recently become a worldwide issue in engineering steels.[1] This failure occurs with the accumulation of cyclic plastic deformation which is generally accompanied with microstructure evolution in a material, such as dislocation multiplication, annihilation and sub-grain initiation. In order to identify the plastic damage and then evaluate the structural health, it is of increasing importance to track the microstructural evolution and then to evaluate the plastic damage of weld joints at an earlier stage. Nondestructive testing and evaluation (NDT & E) techniques such as ultrasonics, eddy-current, thermography, etc. are usually used for the quality assessment of the weld joints.[2] Recently, a nonlinear ultrasonic technique has emerged as a promising tool for NDT & E of the material property degradation,[3–21] such as fatigue, plastic damage, creep, and thermal damage. These references show that the response in harmonics generation can be related to the microstructural change in material.

Now there have been many reports on material assessment of fatigue or plastic deformation using second harmonic generation measurements of ultrasound.[3–21] The influence of a fatigue crack on the harmonic generation was first considered at unbounded interfaces,[7] where the results indicate that the variation of harmonic amplitude could be useful to monitor the state of fatigue. Then, a number of investigators have used nonlinear ultrasonic techniques to assess fatigue damage in different materials, such as plastics and composites,[8] stainless steel,[9] and aluminum alloy.[10] In recent years, there were generally three aspects attracting the attention of fatigue or plastic damage assessment using second harmonic generation measurements. First, various wave types such as surface acoustic wave[11,12] and Lamb waves[13–15] have been used for characterizing the fatigue damage in materials. Second, more exquisite and robust measurement methods such as air-coupled detection[16] have been adopted for ultrasonic measurements. Finally, more analyses of the relationship between second harmonic generation and fatigue/plastic deformation have been presented based on microstructural contributions, including some dislocation-dependent models[17–19] and micrograph-dependent analyses.[20,21] Though recently some investigations of fatigue or plastic deformation in various metallic alloys have been conducted by using nonlinear ultrasound, the systematic work and analysis on plastic damage in complex weld joints are still lacking. Compared with homogeneous materials, e.g. aluminum alloy and titanium alloy, the weld joints have very complex structure, which are

*Project supported by the National Natural Science Foundation of China (Grant Nos. 51325504, 11474093, and 11474361) and the Shanghai Rising-Star Program, China (Grant No. 14QA1401200).

†Corresponding author. E-mail: fzxuan@ecust.edu.cn

© 2016 Chinese Physical Society and IOP Publishing Ltd

more liable to suffer the damage induced by the fatigue/plastic loading.

In addition, most of the previous research focused on the experimental measurements of ultrasonic harmonic generation[11–16] and on the theoretical analyses mainly based on the dislocation monopole model,[22] the dislocation dipole model[10] and other improved models.[18,19] However, less information is available about the numerical analysis of nonlinear ultrasonic response from a damaged material. In fact, numerical simulation could help to provide some valuable insights into the relationship between the nonlinear ultrasonic responses and the degradation of materials. There are some numerical methods available to simulate nonlinearities of media and/or damage, such as finite element method (FEM),[23] finite difference time domain method (FDTD),[24] and local interaction simulation approach (LISA),[25] etc.

In this work, stress-controlled and strain-controlled tensile tests of 30Cr2Ni4MoV martensite weld joints are conducted for fabricating specimens with different plastic deformations, which then are evaluated by the nonlinear ultrasonic technique. The influence of microstructure evolution on the nonlinear ultrasonic responses is also thoroughly analyzed based on metallographic studies, such as transmission electron microscope (TEM). Finally, the commercial finite element analysis software Abaqus is used to simulate the nonlinear ultrasonic waves propagating in the weld region and to verify the correlation between microstructural evolution and the nonlinear ultrasonic measurement.

2. Experimental details

2.1. Specimens preparation

A martensite stainless steel 30Cr2Ni4MoV is used in the study, whose nominal chemical compositions in wt% are listed in Table 1. The weld joint mockup is heat treated at a temperature of (580±10) °C for 10 h and then cooled with a furnace. Flat dog-bone specimens with the welds located in the center are machined from the weld joint mockup, whose nominal dimensions are shown in Fig. 1. From the optical microscopy analysis, it can be identified that the widths of the weld and the heat affected zone (HAZ) are about 20 mm and 2 mm, respectively.

Table 1. Chemical compositions of 30Cr2Ni4MoV stainless steel in wt%.

C	Si	Mn	Cr	Ni	Mo	V	Cu	As	Sn	Fe
≤ 0.35	≤ 0.10	0.20∼0.40	1.50∼2.0	3.25∼3.75	0.25∼0.60	0.07∼0.15	≤ 0.15	≤ 0.02	≤ 0.015	balance

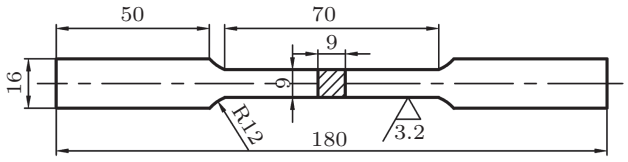


Fig. 1. Dimensions of flat dog-bone specimen of weld joint. All dimensions are in unit mm.

Two sets of plastic deformed specimens are made for experiments using a 100-kN MTS servo hydraulic testing system. One group with 7 specimens are fabricated under stress-controlled mode loading from 774 MPa to 869 MPa (yield strength is 785 MPa), and another one with 5 specimens are fabricated under strain-controlled mode from strain levels of 1.14% to 3.89%. The nonlinear ultrasonic measurements are made off-line after unloading the specimens.

2.2. Nonlinear ultrasonic measurements

Nonlinear ultrasonic measurements are performed on three locations of the specimens, i.e., weld region (about 20 mm in the center), HAZ region (about 2 mm nearing the weld), and the base region. For nonlinear ultrasonic measurement, a Ritec SNAP system with model of RAM-5000 is used to generate the ultrasonic signal. The experimental setup for longitudinal wave measurement is illustrated in Fig. 2,[26] which is primarily composed of the Ritec SNAP system, a high power attenuator, a pre-amplifier, low and high pass filters, transducers, oscilloscope and computer. Amplitudes of the fundamental and second harmonic wave are measured by the transmission method in the present measurements. The cut-off frequencies for the low-pass and high-pass filters are about 6.3 MHz and 9.5 MHz, respectively. A narrow-band longitudinal piezoelectric transducer with a nominal frequency of 5.0 MHz is used to generate the fundamental wave, marked by T. A broad-band 10.0 MHz transducer is used to pick up the receiving signals, denoted by R. The diameters of transmitting and receiving transducers are both 8.6 mm. The transducers T and R are coupled to the specimen by using silicon oil. A special fixture is designed to maintain alignment parallelism between the transmitting and receiving transducers during the whole measurement. A tone burst of ten cycles with a frequency of 5.0 MHz is used to excite the transmitter. The received signal is filtered by a Hanning window and captured by a 300-MHz oscilloscope, and then processed by using an amplitude spectrum fast Fourier transformation (FFT) to extract the amplitudes of the fundamental and second harmonic signals in the frequency domain.

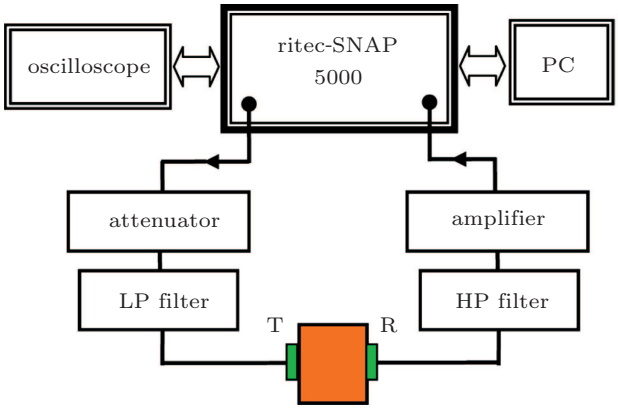


Fig. 2. (color online) Experimental setup for nonlinear ultrasonic measurements.[3]

When exciting a sample by using a single frequency excitation, the second-order nonlinear parameter, known as β, generated by the presence of damaged structure can be expressed as

$$\beta = \frac{8A_{2r}}{k^2 y A_{1r}^2}, \tag{1}$$

where A_{1r} is the real amplitude of the fundamental frequency component, A_{2r} is the real amplitude of the second harmonic component, k is the wave number, and y is the propagation distance. Here, in the following experiments we use a relative acoustic nonlinear parameter (RANP) to characterize the plastic deformation, which is defined as

$$\beta' = \frac{A_2}{A_1^2}, \tag{2}$$

where A_1 is the measured amplitude of the fundamental frequency component and A_2 is the measured amplitude of the second harmonic component.

Figures 3(a) and 3(b) show the variations of the A_2/A_1^2 with loading stress and the plastic strain, respectively. It shows from Fig. 3(a) that the responses of the A_2/A_1^2 versus the loading stress in the three detection regions being measured have the similar tendencies. The measured acoustic nonlinearity exhibits a slight increase in the elastic stage, i.e., the loading stress is less than the yield stress, then it drops as the loading stress slightly exceeds the yield stress, and finally the A_2/A_1^2 shows a monotonic rise with the increase of loading stress. Although the material of the weld region is the same as that of the base, the variation of the A_2/A_1^2 on the location of weld is maximum, nearly three times bigger than the initial value, which means that the plastic-induced deformation of weld would be much more serious than those of HAZ and base regions. Figure 3(b) shows that the A_2/A_1^2 monotonically increases with the plastic strain, which is similar to the change of A_2/A_1^2 in the last stage of Fig. 3(a). Some other previous studies have also reported the same results of the acoustic nonlinearity versus the fatigue or plastic deformation in the engineering materials, such as AA7175-T7351 aluminum alloy[11] and A36 steel.[12]

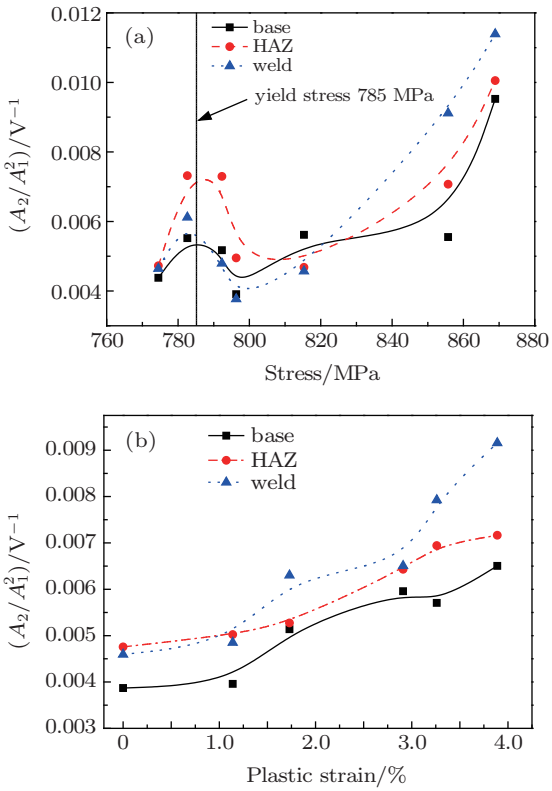


Fig. 3. (color online) Variations of the RANP A_2/A_1^2 with (a) loading stress and (b) plastic strain.

2.3. Microstructural evolution analysis

Microstructure changes of the martensite steel subjected to plastic deformation are thought to originate from the variation of acoustic nonlinearity.[17] Therefore, TEM are used to observe the microstructural evolutions and understand the change of the A_2/A_1^2 with loading stress or plastic strain. Note that the evolution of dislocation in the process of plastic deformation or fatigue damage plays a critical role in the response of acoustic nonlinearity. It is helpful to pay more attention to observing the dislocation multiplication, annihilation and rearrangement during damage. In the following TEM micrograph observation, a Philips CM200 transmission electron microscope is used to take the micrographs. Dislocation density and length are evaluated from the TEM images, in which the density of dislocations is measured by the method of Ref. [27] and the pinning dislocation length is obtained by analyzing the TEM micrographs in computer.

Figure 4 shows the TEM micrographs of 30Cr2Ni4MoV weld joint specimens with different plastic strain levels corresponding to virginal specimen, 1.14% plastic strain, 1.73% plastic strain, and 3.89% plastic strain.[28] Table 2 gives the values of microstructure parameters of the 30Cr2Ni4MoV specimens with different plastic strains, where the dislocation density, length, and dislocation cell size are presented. Note

that each mean value in Table 2 related to dislocations is determined by an average of three to five micrographs from different locations of the specimens. Also, it should be pointed out here that the dislocation cell structures (i.e., the dislocation pile-up) observed in Figs. 4(b)–4(d) would also exert an important influence on the material nonlinearity and whose dislocation density is not easily determined by the method proposed in Ref. [27]. It can be indicated that from Figs. 3 and 4 the evolution of dislocation during the plastic deformation, especially the variation of dislocation density, plays a dominant role in the changing of acoustic nonlinearity. For ease of analysis, it is supposed that the influence of grain or sub-grain evolution of martensite structures on the acoustic nonlinearity is ignored.

Table 2. Microstructure parameters of 30Cr2Ni4MoV weld joint specimens with different plastic strains.

	30Cr2Ni4MoV specimens with different plastic strains/%			
	0	1.14	1.73	3.89
Dislocation density $\Lambda/\times 10^{14}$ m^{-2}	0.35±0.15	1.30±0.26	1.94±0.73	3.70±1.24
Pinning dislocation segment L/μm	0.38±0.042	0.24±0.032	0.20±0.030	0.16±0.010
Applied longitudinal stress σ_0/MPa	60	115	150	200

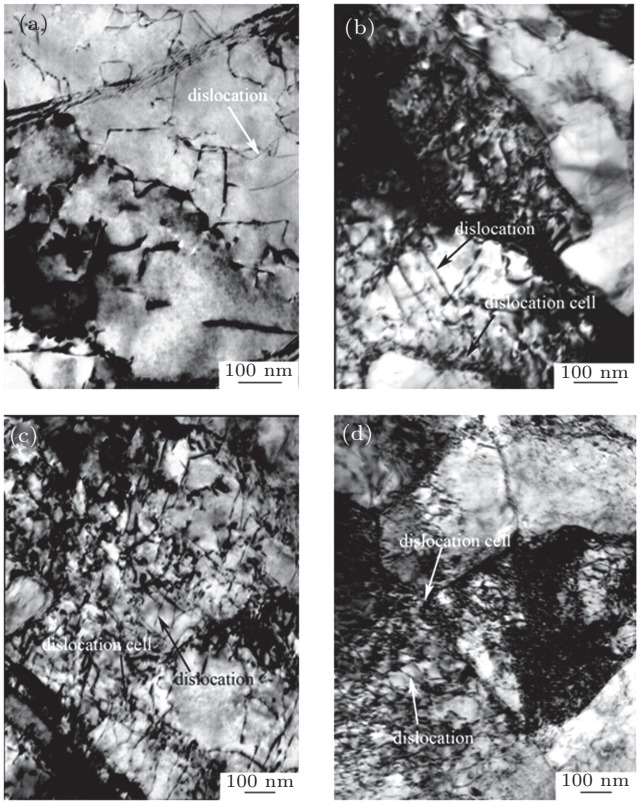


Fig. 4. TEM micrographs of 30Cr2Ni4MoV weld joint specimens with different plastic strain levels: (a) virginal specimen; (b) 1.14% plastic strain; (c) 1.73% plastic strain, and (d) 3.89% plastic strain.[3]

3. Finite element simulations

Finite element simulations are now presented to assist in explaining the experimental results. Consider an isotropic homogeneous solid medium with purely elastic behavior, the nonlinearities of the medium which would contribute to the acoustic nonlinearity may originate from different sources, such as the material and geometric nonlinearities, fatigue- or stress-induced plasticity, etc.

3.1. Fundamental equations of nonlinear elastodynamics

Considering the longitudinal waves in the medium and ignoring the dispersion and attenuation, the equations of motion in the Lagrangian coordinate $\boldsymbol{Y}$ can be written as

$$\rho_0 \frac{\partial^2 u_i}{\partial t^2} = \frac{\partial \sigma_{ij}}{\partial Y_j}, \tag{3}$$

where u_i are the components of the particle displacement vector, and the stresses σ_{ij} are the components of the first Piola–Kirchhoff tensor, and ρ_0 is the mass density in the unstressed state.

The stress tensor in Eq. (3) may be expanded in terms of the particle displacement gradients as[29]

$$\begin{aligned}\sigma_{ij} &= C_{ijkl}\frac{\partial u_k}{\partial Y_l} + \frac{1}{2}(C_{ijklmn} + C_{ijln}\delta_{km} \\ &\quad + C_{jnkl}\delta_{im} + C_{jlmn}\delta_{ik})\frac{\partial u_k}{\partial Y_l}\frac{\partial u_m}{\partial Y_n},\end{aligned} \tag{4}$$

where C_{ijkl} and C_{ijklmn} are the components of the second- and third-order elastic tensors defined as

$$C_{ijkl} = \lambda\delta_{ij}\delta_{kl} + 2\mu I_{ijkl}, \tag{5}$$

$$\begin{aligned}C_{ijklmn} &= \frac{A}{2}\left(\delta_{ik}I_{jlmn} + \delta_{il}I_{jkmn} + \delta_{jk}I_{ilmn} + \delta_{jl}I_{ikmn}\right) \\ &\quad + 2B\left(\delta_{ij}I_{klmn} + \delta_{kl}I_{mnij} + \delta_{mn}I_{ijkl}\right) \\ &\quad + 2C\delta_{ij}\delta_{kl}\delta_{mn},\end{aligned} \tag{6}$$

where λ and μ are the Lamé parameters; A, B, and C are the third-order elastic (TOE) constants in isotropic media, which are related to the inherent properties of the material; δ_{ij} are the Kronecker's deltas; $I_{ijkl} = \left(\delta_{ik}\delta_{jl} + \delta_{il}\delta_{jk}\right)/2$. Note that C_{ijklmn} can be expressed explicitly with Voigt notation in terms of the three TOE constants A, B, and C. It also should be pointed out that in Eq. (4), the C_{ijkl} is associated with the linear property of material, and the term of $C_{ijln}\delta_{km} + C_{jnkl}\delta_{im} + C_{jlmn}\delta_{ik}$ is associated with the geometric nonlinearity that is

caused mainly by the mathematic transform between the Eulerian (spacial) coordinates and Lagrangian (material) coordinates, and then C_{ijklmn} is the TOE tensors describing the material nonlinearity. Hence, the second term on the right-hand side in Eq. (4) introduces the nonlinear effect on the medium.

Considering a one-dimensional medium such as a rod, the wave solution of Eq. (3) can be obtained by a simple perturbation analysis as

$$u(Y_1,t) = u_0 \sin(kY_1 - \omega t) + \frac{u_0^2 k^2 \beta_{\rm I} Y_1}{8} \cos 2(kY_1 - \omega t), \quad (7)$$

where u_0 is the amplitude of the fundamental wave, k is the wave number, ω is the angular frequency of excitation, $u_0^2 k^2 \beta_{\rm I} Y_1/8$ is the amplitude of the second harmonic wave with $\beta_{\rm I}$ denoting the acoustic nonlinearity parameter of the medium at the intact state.

For a medium experiencing plastic deformation, localized plasticity damage would appear in the form of microstructural defects such as dislocations, which could be a source of nonlinearity for the wave propagation. In contrast to $\beta_{\rm I}$, another nonlinearity parameter $\beta_{\rm D}$ is defined to describe the plasticity-induced nonlinearity for the damage state of the material. For ease of numerical simulation, here we restrict discussion to the dislocation monopoles contributing to the nonlinear parameters of the material, which can be expressed as[22,30]

$$\beta_{\rm D} = \frac{24}{5} \frac{\Omega \Lambda L^4 R^3 (\lambda + 2\mu)^2}{\mu^3 b^2} |\sigma_0| \propto \Lambda L^4 |\sigma_0|, \quad (8)$$

where Λ is the dislocation density, L is the dislocation length, b is the Burgers vector, R is the resolving shear factor, Ω is the conversion factor from shear strain to longitudinal strain, $|\sigma_0|$ is the magnitude of the initial residual or internal longitudinal stress in the material, and σ_0 can be obtained from $\sigma_0 = \alpha \mu b \sqrt{\Lambda}$,[20,28] with α being a constant that is defined to be in a range from 0 to 1.0.

Therefore, the acoustic nonlinearity parameter β of Eq. (1) which can be calculated from the experimental measurement or numerical simulation usually comes from the total contributions of $\beta_{\rm I}$ and $\beta_{\rm D}$.

3.2. Numerical simulation details

Based on the above analyses of the nonlinear elastodynamics, a finite element simulation is conducted in an attempt to explain the variation of acoustic nonlinearity in the plasticity deformed material, which is developed and carried out on the basis of the commercial FEM software Abaqus/EXPLICIT. The intact state and plastic-damaged state with dislocations in materials are taken into account in the following FEM models.

The numerical simulation of material, geometric, and plasticity-induced nonlinearities is performed by introducing the nonlinear stress-strain constitutive relation (i.e., Eq. (4)) to Abaqus/EXPLICIT through the interface of user subroutine VUMAT, which can be used for material definition and called in the iteration of the program. A two-dimensional (2D) model is established to simulate the longitudinal wave propagating in the weld joints, whose schematic of 2D model is shown in Fig. 5 with the same dimensions as the experimental samples. The wave generation is excited by imposing longitudinal (y axis) stress loadings with a ten-cycle Hanning-windowed sinusoidal tone burst at 5.0 MHz and an input acoustic pressure amplitude of 20 MPa, whose loading size is 8.6 mm, similar to the diameter of the transducer. The signal (longitudinal stress, S22 in Abaqus system) is picked through the middle node of the bottom edge as shown in Fig. 5. The second-order elastic constants of Lamé parameters λ and μ in 30Cr2Ni4MoV are assumed to be 116 GPa and 84 GPa, respectively. The TOE constants of the material used here are as follows: $A = 1100$ GPa, $B = -1580$ GPa, and $C = 1230$ GPa.[31]

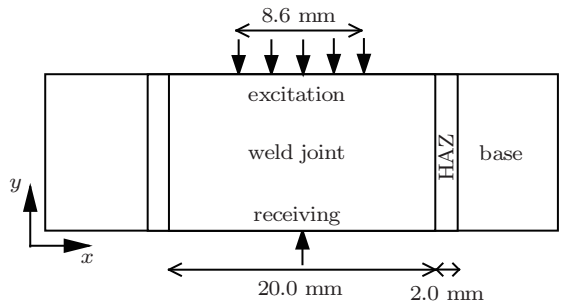


Fig. 5. Schematic diagram of the simulation model for longitudinal wave propagating in weld joint.

The four-node reduced-integration plane strain elements (CPE4R) in Abaqus are used to mesh the rectangular model through a structured meshing algorithm, whose elements are equally sized at 0.05 mm (Δy) with a spatial resolution of $\lambda_{\rm L}/24$ where $\lambda_{\rm L}$ is the wavelength of the fundamental wave (about 1.2 mm). This spatial resolution is chosen to warrant simulation precision and error convergence. According to the Fourier or von Neumann stability analysis,[32] the time step Δt should be smaller than the time required for the longitudinal wave to travel across the element length, that is,

$$\Delta t \leq \frac{\Delta y}{c_{\rm L}}, \quad (9)$$

where $c_{\rm L}$ is the longitudinal wave velocity. In this simulation, a fixed time step of 2.626×10^{-9} s is set to guarantee an effective and stable calculation in the simulations for the intact state material.

A snapshot of the ultrasonic wave (in the form of stress contour) propagating in the weld joint is shown in Fig. 6. The results for three simulations corresponding to three variants of the stress-strain constitutive relation (Eq. (4)) are presented as follows.

(i) Linear elastic material (LEM)

Without material and geometric nonlinearities, i.e., $A = B = C = 0$ and the term of $C_{ij\ln}\delta_{km} + C_{jnkl}\delta_{im} + C_{jlmn}\delta_{ik}$ equals zero.

(ii) Geometrically nonlinear material (GNM)

Only geometric nonlinearity is considered, i.e., $A = B = C = 0$ and the term of $C_{ij\ln}\delta_{km} + C_{jnkl}\delta_{im} + C_{jlmn}\delta_{ik}$ is used in the strain measure.

(iii) Nonlinear material (NLM)

Both material and geometric nonlinearities are considered, i.e., $A \neq 0$, $B \neq 0$, $C \neq 0$ and the term of $C_{ij\ln}\delta_{km} + C_{jnkl}\delta_{im} + C_{jlmn}\delta_{ik}$ is used in the strain measure.

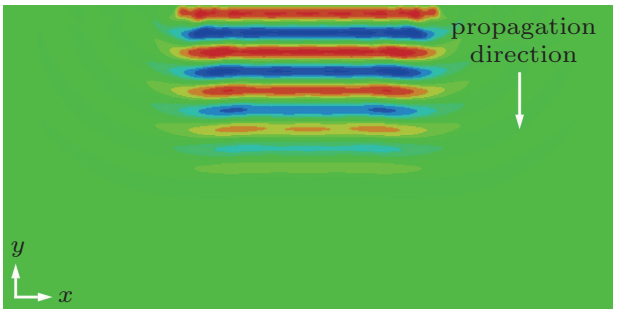


Fig. 6. (color online) A snapshot of the ultrasonic wave propagating in the weld joint (in the form of stress contour).

According to the above different conditions of (i)–(iii), figure 7 shows the signals of frequency domain for the three cases, in which it can be seen that there is very little difference for the fundamental wave at 5.0 MHz but an obvious change for the second harmonic wave (or nonlinearity). Note that the 'LEM' case shows no second harmonic component as Eq. (4) describes (the first term on the right-hand side in the equation) and the other two cases have evident second harmonic components. It is also interesting to see that the amplitude of the second harmonic generated in the 'NLM' case is about 4.3 times greater than that generated in the 'GNM' case, as also reported in Ref. [23], which means that the material nonlinearity may play a dominant role in the generating of the second harmonics. In the following studies, only the 'NLM' case will be considered in all of the simulation implementations.

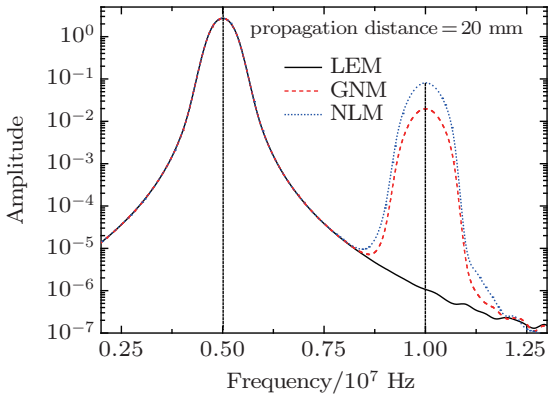


Fig. 7. (color online) Frequency domain signals obtained using LEM, GNM, and NLM stress–strain constitutive models.

3.3. Numerical simulation implementations of weld region

Prior to the numerical simulations, some assumptions should be made for the simulations of plastic-damaged state with dislocations in material. First, only plastic-induced edge dislocations are taken into account in the following simulations just as shown in Fig. 4. According to the dislocation string model presented by Hikata *et al.*,[22,30] the change of the acoustic nonlinear parameter resulting from the bowing out of a pinned dislocation under a stress σ_0 can be given by Eq. (8). So, a pinned string (or line) is used to simulate the monopole dislocation in Abaqus system. Second, the pinned string is perpendicular to the direction of wave motion and located in the middle of the simulation area. In addition, the dislocation density is small so that the interaction between dislocations can be ignored.

It can be seen from the microstructural analysis of Subsection 2.3 and Table 2 that the lengths of the pinned dislocations vary from 0.38 μm to 0.16 μm when the 30Cr2Ni4MoV is subjected to plasticity deformation. Therefore, in order to approximately simulate monopole dislocation in Abaqus, the element length should be reduced at least to 0.05 μm that is smaller than dislocation length. For saving computing time and space, localized refined mesh (LRM) with an area of 20 μm×10 μm and an element length of 0.05 μm is adopted in FEM model described in Subsection 3.2 (here it is called regular model) to model the damaged state with dislocation in the following simulations as shown in Fig. 8. The transition grid is used for the LRM to reduce the element length from 0.05 mm to 0.05 μm as shown in the circled region in Fig. 8. Note that the time step Δt should also satisfy the condition of Eq. (9), and then an auto-increase increment of time step from 5.25×10^{-12}s to 7.19×10^{-12} s is set to guarantee a stable calculation in the simulations for the damaged material.

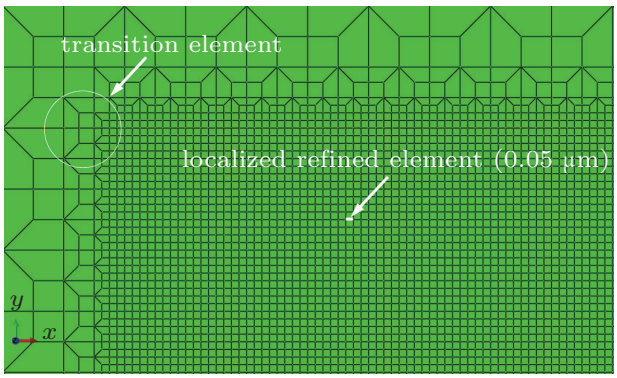


Fig. 8. (color online) Meshed structure with localized refined mesh (LRM) and a minimum element length of 0.05 μm formed by using transition element.

Three examples of numerical simulations for dislocations with different pinned lengths such as 0.2 μm, 0.3 μm, and 0.4 μm are demonstrated, corresponding to the really measured dislocation lengths as given in Table 2.

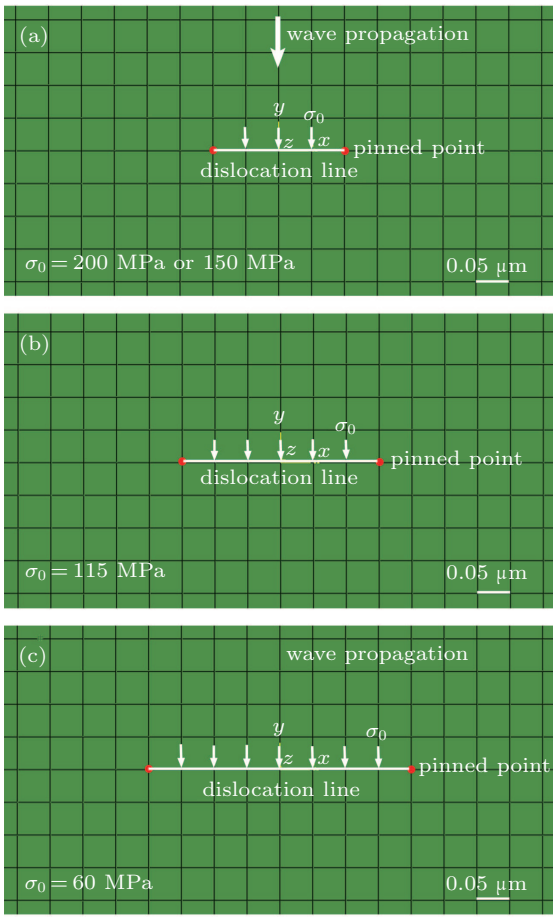


Fig. 9. (color online) configurations of the dislocation located in the middle of the LRM model, in which pinned strings are used for modeling different dislocations in the damaged states: (a) 0.2 μm, (b) 0.3 μm, and (c) 0.4 μm. The solid circles represent the pinned points of dislocations with a zero displacement.

Figure 9 shows the configurations of the dislocations located in the middle of the LRM model, in which the displacement of the two pinned points is fixed and set to be zero and the different values of internal stress σ_0 are applied to the nodes of the dislocation line (the values of applied stress can be found in Table 2). All of the other set-up parameters such as excitation condition, loading area and receiving point are the same as those set in Subsection 3.2. Then, the influences of dislocations with different lengths on the response of wave motion can be seen from the frequency domain as shown in Fig. 10. It is noted that although the variation of the receiving signal caused by one dislocation is tiny, the corresponding A_2/A_1^2 monotonically increases with σL^4 as expected in Eq. (8), which is listed in Table 3.

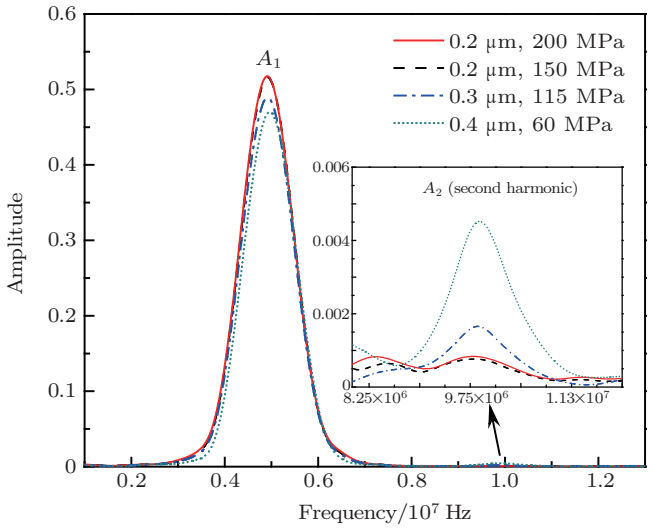


Fig. 10. (color online) Amplitudes of the fundamental (A_1) and second-harmonic (A_2) in the frequency domain for simulation of dislocations with different lengths.

Table 3. Values of dislocation simulation for the plastic deformed materials.

	The results obtained by LRM model simulation for one dislocation with different lengths L/μm			
	0.4	0.3	0.2	0.2
Fundamental A_1/MPa	0.470	0.489	0.516	0.518
Second harmonic A_2/MPa	0.004662	0.001645	0.000765	0.000787
(A_2/A_1^2)/MPa^{-1}	0.02111	0.00686	0.002873	0.002933
Corresponding plastic strain in experiments	0%	1.14%	1.73%	3.89%
Corresponding Λ in experiments by TEM/10^{14} m^{-2}	0.35	1.30	1.94	3.70
Normalization of nonlinearity parameter caused by plastic strain, Eq. (10)	1	1.207	0.754	1.468

4. Results and discussion

4.1. Results of dislocation simulation

From Figs. 9 and 10 and Table 3, it can be seen that although the numerical calculation of A_2/A_1^2 monotonically increases with dislocation length, the results are not exactly proportional to the value of σL^4 as described in Eq. (8). In fact, compared with the sophisticated analytical models, here the simple approximation of modeling a single pinned monopole dislocation as a pinned string perpendicular to the direction of wave motion seems to yield the results of A_2/A_1^2 proportional to σL^n, where $n = 3$–5.

Note that the above established LRM model represents the damaged state only with one dislocation. Here, in order to extend a one-dislocation result into multi-dislocation state

to simulate the practical specimens conducted in the experiments, we can make a correlation of β_D with the simulation result of one-dislocation A_2/A_1^2 and the corresponding dislocation density Λ as

$$\beta_D = \beta - \beta_I \propto \Lambda \frac{A_2}{A_1^2}\bigg|_{one-dislocation}. \quad (10)$$

Then, the term on the right-hand side of Eq. (10) is normalized by the maximum value, as shown in the last line of Table 3, which can be used to describe the variation of nonlinearity response due to the plasticity damage.

4.2. Comparison between experimental and FEM simulation results

Figure 11 shows the values of A_2/A_1^2 normalized by their corresponding initial values, each as a function of the plastic strain for experimental measurement (the measured data of weld zone under stain-controlled mode) and FEM simulation, respectively. The error bars of the standard deviation are determined by repeating the measurements five times. It is worth noting that the result of FEM in Fig. 11 represents the acoustic nonlinear response caused by plastic damage as described by Eq. (8), whereas the experimental result refers to the total acoustic nonlinearity, i.e., β. According to the previous studies,[8–11] the damage-induced material nonlinearity generally plays a dominant role in the acoustic nonlinearity response. Therefore, it is reasonable to make an approximation i.e., $\beta \approx \beta_D$ in the process of damage loading, especially in the late stage. So, it leads to a good comparability between the experimental result and FEM simulation result after being normalized. From Fig. 11, it is clear that the change tendency of the normalized nonlinear parameter obtained from experimental measurement is in good accordance with that calculated by FEM model, except the third solid circle.

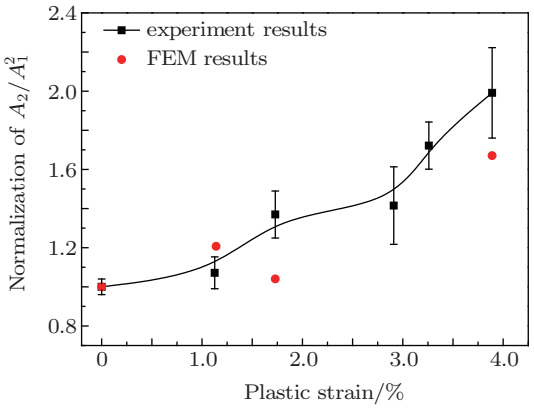


Fig. 11. (color online) Normalized A_2/A_1^2 values each as a function of plastic strain for experimental measurement and FEM simulation respectively.

However, the calculated results from the FEM model are underestimated compared with those measured results, especially in the late stage. In this perspective, there may be other microstructures that would contribute to the acoustic nonlinearity during the plastic strain loading, such as the dislocation cells or walls, as marked by arrows in Fig. 4. However, the influence of a dislocation cell on the acoustic nonlinearity has not been considered in this FEM simulation because of lacking proper models to measure the dislocation cell density and to describe the correlation with the acoustic nonlinearity. Another reason for the underestimation of FEM results maybe is due to the fact that the contributions of the mixed dislocations including edge dislocation and screw dislocation to the acoustic nonlinearity have not been considered here in FEM model, which as reported[19,28] plays a positive influence on the increase of nonlinear parameter β.

5. Conclusions

In this article the experimental measurement and numerical simulation are performed to study the ultrasonic nonlinear responses from the plastic deformation in 30Cr2Ni4MoV weld joints. The measurement results show that the normalized nonlinear parameter A_2/A_1^2 monotonically increases with the plastic strain, and that the variation of A_2/A_1^2 in the weld region is maximum, nearly being a 200% change in nonlinear parameter, which means much more serious plasticity damage here than those of HAZ and base regions. Microscopic images of TEM relating to the microstructure evolution of the weld region are studied to explain the change tendency of the measured A_2/A_1^2, which reveals that the variation of A_2/A_1^2 is mainly attributed to the dislocation evolutions in the process of plastic deformation loading.

Meanwhile, an FEM model is presented to investigate the behavior of nonlinear wave propagation associated with material and plastic damage, which is carried out by introducing the nonlinear stress-strain constitutive relation to Abaqus through the interface of user subroutine VUMAT. The modeling technique focuses on material, geometric and plasticity-induced nonlinearities that may contribute to the variation of acoustic nonlinearity. A pinned string model is used to simulate dislocation evolution (0.2 μm–0.4 μm) during the plastic damage. Results from the simulation and the experiments show that they are in good consistency with each other, both reveal a rising acoustic nonlinearity due to the variation of the dislocation length and density. The FEM model developed here could be a good supplementary way to provide insights into the nonlinear wave propagation and its interaction with the dislocations, precipitates and micro-voids or micro-cracks in materials.

References

[1] Watanabe T, Tabuchi M, Yamazaki M, Hongo H and Tanabe T 2006 *Int. J. Pressure Vessels Piping* **83** 63
[2] Sposito G, Ward C, Cawley P, Nagy P B and Scruby C 2010 *NDT & E Int.* **43** 555

[3] Xiang Y X, Deng M X and Xuan F Z 2014 *J. Nondestruct. Eval.* **33** 279

[4] Kim C S and Jhang K Y 2012 *Chin. Phys. Lett.* **29** 060702

[5] Deng M X and Xiang Y X 2010 *Chin. Phys. B* **19** 114302

[6] Xiang Y X, Deng M X, Xuan F Z and Liu C J 2011 *Ultrasonics* **51** 974

[7] Buck O, Morris W L and Richardson J M 1978 *Appl. Phys. Lett.* **33** 371

[8] Nagy P B 1998 *Ultrasonics* **36** 375

[9] Jhang K Y and Kim K C 1999 *Ultrasonics* **37** 39

[10] Cantrell J H and Yost W T 2001 *Int. J. Fatigue* **23** 487

[11] Rao V V S J, Kannan E, Prakash R V and Balasubramaniam K 2009 *Mater. Sci. Eng. A* **512** 92

[12] Walker S V, Kim J Y, Qu J and Jacobs L J 2012 *NDT & E Int.* **48** 10

[13] Deng M X and Pei J F 2007 *Appl. Phys. Lett.* **90** 121902

[14] Pruell C, Kim J Y, Qu J and Jacobs L J 2007 *Appl. Phys. Lett.* **91** 231911

[15] Xiang Y X and Deng M X 2008 *Chin. Phys. B* **17** 4232

[16] Thiele S, Kim J Y, Qu J and Jacobs L J 2014 *Ultrasonics* **54** 1470

[17] Cantrell J H 2006 *J. Appl. Phys.* **100** 063508

[18] Zhang J F, Xuan F Z and Xiang Y X 2013 *Europhys. Lett.* **103** 68003

[19] Cash W D and Cai W 2011 *J. Appl. Phys.* **109** 014915

[20] Oruganti R K, Sivaramanivas R, Karthik T N, Kommareddy V, Ramadurai B, Ganesan B, Nieters E J, Gigliotti M F, Keller M E and Shyamsunder M T 2007 *Int. J. Fatigue* **29** 2032

[21] Kumar A, Torbet C J, Jones J W and Pollock T M 2009 *J. Appl. Phys.* **106** 024904

[22] Hikata A, Chick B B and Elbaum C 1965 *J. Appl. Phys.* **36** 229

[23] Chillara V K and Lissenden C J 2014 *Ultrasonics* **54** 1553

[24] Matsuda N and Biwa S 2012 *Jpn. J. Appl. Phys.* **51** 07GB14

[25] Lee B C and Staszewski W J 2007 *Smart Mater. Struct.* **16** 249

[26] Xiang Y X, Zhu W J, Liu C J, Xuan F Z, Wang Y N and Kuang W C 2015 *NDT & E Int.* **72** 41

[27] Pešička J, Kužel R, Dronhofer A and Eggeler G 2003 *Acta Mater.* **51** 4847

[28] Xiang Y X, Deng M X, Liu C J and Xuan F Z 2015 *J. Appl. Phys.* **117** 214903

[29] Norris A N 1998 *Nonlinear Acoustics* (Hamilton M and Blackstock D eds.) (San Diego CA: Academic Press) pp. 263–264

[30] Cantrell J H and Yost W T 2000 *Appl. Phys. Lett.* **77** 1952

[31] Shui Y and Solodov I Y 1988 *J. Appl. Phys.* **64** 6155

[32] Sewell G 2005 *The numerical solution of ordinary and partial differential equations*, 2nd edn. (New Jersey: John Wiley and Sons Inc.) pp. 53–54